FGFR2 fusion proteins drive oncogenic transformation of mouse liver organoids towards cholangiocarcinoma

Short title*: FGFR2 fusions in cholangiocarcinoma models*

Giulia Cristinziano[1], Manuela Porru[1], Dante Lamberti[1], Simonetta Buglioni[2], Francesca Rollo[2], Carla Azzurra Amoreo[2], Isabella Manni[3], Diana Giannarelli[4], Cristina Cristofoletti[5], Giandomenico Russo[5], Mitesh J. Borad[6], Gian Luca Grazi[7], Maria Grazia Diodoro[3], Silvia Giordano[8,9], Andrea Sacconi[4], Mattia Forcato[10], Sergio Anastasi[1]*, Carlo Leonetti[2]* and Oreste Segatto[1]*

[1]Unit of Oncogenomics and Epigenetics, IRCCS Regina Elena National Cancer Institute, Rome, Italy

[2]Department of Pathology, IRCCS Regina Elena National Cancer Institute, Rome, Italy

[3]SAFU, IRCCS Regina Elena National Cancer Institute, Rome, Italy

[4]UOSD Clinical Trial Center, Biostatistics and Bioinformatics, IRCCS Regina Elena National Cancer Institute, Rome, Italy

[5]Istituto Dermopatico dell'Immacolata, IDI-IRCCS, Rome, Italy

[6]Division of Hematology and Oncology, Mayo Clinic, Scottsdale, USA

[7]Division of Hepatobiliary Pancreatic Surgery, IRCCS Regina Elena National Cancer Institute, Rome, Italy

[8]Department of Oncology, University of Torino, Candiolo, Italy

[9]Candiolo Cancer Institute, FPO-IRCCS, Candiolo, Italy

[10]Center for Genome Research, Dept. of Life Sciences, University of Modena and Reggio Emilia, Modena, Italy

*****Corresponding Author

Please address correspondence to:

Oreste Segatto, MD
Unit of Oncogenomics and Epigenetics,
IRCCS Regina Elena National Cancer Institute,

via E. Chianesi, 53
00144 Rome, Italy
Ph. 39-0652662551
oreste.segatto@ifo.gov.it

Carlo Leonetti, PhD
SAFU
IRCCS Regina Elena National Cancer Institute,
via E. Chianesi, 53
00144 Rome, Italy
Ph. 39-0652662534
carlo.leonetti@ifo.gov.it

Sergio Anastasi, PhD
Unit of Oncogenomics and Epigenetics,
IRCCS Regina Elena National Cancer Institute,
via E. Chianesi, 53
00144 Rome, Italy
Ph. 39-0652662568
sergio.anastasi@ifo.gov.it

Keywords: cholangiocarcinoma, BGJ398, mouse models, FGFR2 fusions, liver organoids, targeted therapies, FGFR2-BICC1, FGFR2 gatekeeper mutation, trametinib

All Authors, except M.J.B., have no personal, professional or financial conflicts to disclose.

M.J.B. disclosures: ADC Therapeutics – Consulting to self; Exelixis Pharmaceuticals – Consulting to self; Inspyr Therapeutics – Consulting to self; G1 Therapeutics – Consulting to self; Immunovative Therapies – Consulting to self; OncBioMune Pharmaceuticals – Consulting to self; Western Oncolytics – Consulting to self; Lynx Group – Consulting to self; Genentech – Consulting to self; Merck – Consulting to self; Huya – Consulting to self; Astra Zeneca – Travel Support to self

Grant support: O. Segatto is funded by AIRC (IG2018, ID 21627, PI Segatto Oreste) and an intramural grant-in-aid funded by the Italian Ministry of Health.

Authors' contributions

G.C.: investigation, methodology, writing of manuscript draft

M.P.: investigation, methodology

D.L., F.R., C.A.A., I.M.: investigation

S.B.: conceptualization, investigation, methodology

D.G.: formal analysis, methodology

C.C.: formal analysis, investigation, methodology

G.R.: resources, writing

M.J.B.: resources, writing

G.L.G.: conceptualization

M.G.D.: formal analysis

S.G.: conceptualization, methodology, writing of manuscript

A.S. formal analysis, investigation

M.F.: data curation, formal analysis, investigation, methodology

S.A.: investigation, supervision, writing of manuscript

C.L.: formal analysis, methodology, supervision, writing of manuscript

O.S.: conceptualization, formal analysis, funding acquisition, supervision, writing of manuscript

Abstract

Background and aims. About 15% of intrahepatic cholangiocarcinoma (iCCA) express fibroblast growth factor receptor 2 (FGFR2) fusion proteins (FFs), most often in concert with mutational inactivation of *TP53*, *CDKN2A* or *BAP1*. In FFs, FGFR2 residues 1-768 are fused to sequences encoded by a diverse array of partner genes (>60), a configuration that causes oncogenic FF activation. While FGFR-specific tyrosine kinase inhibitors (F-TKI) provide clinical benefit in FF^+ iCCA, responses are partial and/or limited by resistance mechanisms, including FF tyrosine kinase domain mutations, such as the V565F substitution in the FGFR2 gatekeeper residue. Improving on FF targeting in iCCA therefore remains a critical and unmet need. Herein, we present the generation of FF-driven murine iCCA models and their exploitation for discovering actionable FF-associated dependencies.

Methods. Four iCCA FFs carrying different fusion sequences were expressed in *Tp53*$^{-/-}$ mouse liver organoids. Tumorigenic properties of genetically modified liver organoids were assessed by transplantation in immuno-deficient mice. Cellular models derived from neoplastic lesions were exploited for pre-clinical studies.

Results. Transplantation of FF-expressing liver organoids yielded tumors diagnosed as CCA based on histological, phenotypic and transcriptomic analyses. The penetrance of this tumorigenic phenotype was influenced by FF identity. Tumor organoids and 2D cell lines derived from CCA lesions were addicted to FF signaling via Ras-Erk, regardless of FF identity or V565F mutation. Dual blockade of FF and Ras-Erk pathway by concomitant pharmacological inhibition of FFs and Mek1/2 provided greater therapeutic efficacy than single agent F-TKI *in vitro* and *in vivo*.

Conclusions. FF-driven iCCA pathogenesis was successfully modeled in murine *Tp53*$^{-/-}$ background, revealing biological heterogeneity among structurally different FFs. Double blockade of FF-Erk signaling deserves consideration for precision-based approaches against human FF^+ iCCA.

Abbreviations used in this paper

ANOVA, analysis of variance; Bap1, BRCA1-Associated-Protein 1; CAA, cholangiocarcinoma; Cdkn2a, cyclin-dependent kinase inhibitor 2A; EGF, epidermal growth factor; EGFR, epidermal growth factor receptor; EpCAM, epithelial cell adhesion molecule; Erk, extracellular signal–regulated kinase; FGFR2, fibroblast growth factor receptor 2; FRS2, fibroblast growth factor receptor substrate 2; GRB2, growth factor receptor-bound 2; GSEA, gene set enrichment analysis; GSVA, gene set variation analysis; H&E, hematoxylin and eosin; HCC, hepatocellular carcinoma; HepPar1, hepatocyte Paraffin 1; Lgr5, leucine-rich repeat-containing G-protein coupled receptor 5; MSigDB, Molecular Signature Database; NTRK, neurotrophic Tyrosine Kinase; Parp, Poly (ADP-ribose) polymerase; RECIST, response evaluation criteria in solid tumors; SHP2, Src homology phosphatase 2; TCGA, the cancer genome atlas; TME, tumor microenvironment.

Introduction

Large scale sequencing studies have identified actionable genomic drivers in intrahepatic cholangiocarcinoma (iCCA), raising hopes for transformative approaches to this still largely incurable disease[1]. In particular, chromosomal rearrangements that give rise to FGFR2 fusion proteins were reported to occur in 12-15% of iCCA patients[2]. As depicted in Fig. S1, iCCA FGFR2 fusion proteins, henceforth referred to as FFs, contain residues 1-768 of FGFR2IIIb fused to sequences encoded by any of a long list of partner genes (>60 identified so far)[3,4]. It is thought that the fusion partner forces constitutive dimerization of adjacent FGFR2 sequences, triggering constitutive activation of the FGFR2 tyrosine kinase domain (TKD) and attendant oncogenic signaling[3]. However, it is unknown whether FFs are sufficient to initiate iCCA pathogenesis. Whether different fusion sequences may bestow specific oncogenic properties onto FFs remains an unresolved issue[1].

Meaningful clinical responses have been observed (~25-35% response rate) in FF^+ iCCA patients treated with FGFR-specific tyrosine kinase inhibitors (F-TKI), including BGJ398, TAS-120 and pemigatinib[1], all of which have now progressed to phase 3 clinical experimentation as first-line single agents in FF^+ iCCA[1]. While providing a proof of principle that FFs are actionable iCCA oncogenic drivers, the above studies highlighted that clinical responses to FF targeting in iCCA are most often of modest durability. Although mechanisms of primary resistance remain unknown[1], a number of mutations causing single aminoacid substitutions in the FF TKD were found to be a genetic determinant of secondary resistance, due to their ability to impair drug-target interactions[5-7]. Additional routes to F-TKI resistance, likely linked also to non-genetic mechanisms, are postulated to exist in FF^+ iCCA[5-7]. It therefore appears that further progress towards therapeutic targeting of FF^+ iCCA requires the implementation of novel and more aggressive pharmacological approaches.

A significant hurdle to this strategy is the lack of readily and widely available genetically defined iCCA models suitable for pre-clinical investigation. Recent studies have shown that primary liver

tumors can be modeled using liver organoids[8-11], i.e. 3D cultures of bipotent liver precursors, which can be manipulated *in vitro* to create the desired cancer-driving genetic make-up and subsequently transplanted in mice to allow for tumor development[5,8,9,11]. In these models, specific oncogenes, e.g. MYC and KRAS, caused hepatocellular carcinoma (HCC) and iCCA, respectively, in a mutually exclusive manner[8,11]. This obligate lineage commitment recapitulated the role played by MYC and RAS as select drivers of HCC and iCCA in human liver cancer and appeared to be instructed by oncogene-specific cell intrinsic cues, at least in some models[11]. Herein, we report that structurally different FGFR2 fusions were sufficient to drive oncogenic conversion of *Tp53*-null mouse liver organoids towards cholangiocarcinoma and exploited this model for pre-clinical pharmacological targeting of FGFR2 fusions.

Materials and methods

Details on cell culture procedures and media, viral vectors, gene transfer procedures, immunoblotting, immunofluorescence, histopathology and immunohistochemistry are included in Supplementary information along with the list of reagents, antibodies, PCR primers and kits (Tables S1-4). Requests for reagents and additional details should be addressed to O.S.

Animal studies

All animal experimentation procedures were approved by the ethics committee of the Regina Elena National Cancer Institute (code 12048) and the Italian Ministry of Health (codes 947/2015-PR and 409/2019-PR) and were in compliance with the national and international directives (D.L. March 4, 2014, no. 26; directive 2010/63/EU of the European Parliament and European Council; Guide for the Care and Use of Laboratory Animals, United States National Research Council, 2011; Animal Research guidelines Reporting of *In Vivo* Experiments (ARRIVE) guidelines). Further details on organoid tumorigenicity assays, tumor imaging, pharmacological experiments in tumor-bearing mice and data analysis/quantification are provided in Supplementary materials and methods.

Statistical analysis

Values were expressed as average ± SEM. One-way analysis of variance (ANOVA) with a post hoc Bonferroni's test was used for multiple sample comparisons. The student's t-test (unpaired, two-tailed) was used for single pair-wise comparisons. Differences were considered statistically significant when $P < 0.05$. Data were elaborated using GraphPad Prism Software 8.3.

Results

Generation of mouse liver organoids expressing FGFR2 fusion proteins

Organoids derived from livers explanted from adult C57BL/6J mice developed as buds extending from biliary ducts, as reported[12,13]. Upon passaging, these outgrowths yielded homogeneous cultures of spherical cysts (Fig. S2A), that expressed the stem cell marker *Lgr5* along with markers of both hepatocyte and cholangiocellular lineages, as described[12,13] (Fig. S2B). Three structurally different FFs previously identified in iCCA, namely the highly recurrent FGFR2-BICC1 and the sporadic FGFR2-MGEA5 and FGFR2-TACC3 fusions[14,15] (henceforth abbreviated as F-BICC1, F-MGEA5 and F-TACC3 in the main text or F-B, F-M and F-T in figures) were individually expressed in liver organoids derived from wild type C57BL/6J mice. Ectopic FFs caused a dramatic reduction of organoid growth, compared to controls infected with empty virus. This phenotype was rescued by dose-dependent reduction of *Tp53* (Fig. 1A and Fig. S2C, D), which most likely alleviated the oncogenic stress caused by unabated FF signaling (see below). In line with this observation, mutations affecting tumor suppressor genes (TSGs), most notably *TP53*, *CDKN2A* or *BAP1*, co-occur in the large majority of iCCA carrying FGFR2 fusions[14,16]. *Tp53*$^{-/-}$ organoids expressing F-BICC1, F-MGEA5 and F-TACC3 (the latter in either wt or TKI-resistant V565F configuration[17]) yielded tag-specific reactivity (GFP-tagged F-MGEA5 and F-TACC3; MYC-tagged F-BICC1 and F-TACC3 V565F) (Fig. 1B), that, in agreement with FFs being exposed at the cell surface[17], outlined the cell periphery (see also Fig. S2E). Immunoblot analysis confirmed expression and constitutive phosphorylation of FFs in transduced organoids, with F-BICC1 being expressed at lowest levels (Fig. 1C). Notably, when expressed at levels comparable to those of F-TACC3, wt FGFR2IIIb required ligand stimulation in order to undergo catalytic activation (Fig. 1D). Thus, constitutive FF signaling in the above liver organoid models is caused by the ligand-independent mode of activation typical of iCCA FGFR2 fusions[3]. Compared to control organoids, FF expression did not cause obvious alterations of *Lgr5* and lineage markers (Fig. S2B).

Despite their constitutive activation, FGFR2 fusions did not confer *in vitro* growth advantage, even under conditions of growth factor deprivation. Along these lines, FF inhibition by BGJ398, a clinically advanced F-TKI[18], did not cause growth inhibition of FF-expressing liver organoids (Fig. S3A, B). The observation that FFs lacked an obvious growth-promoting effect in the *Tp53*$^{-/-}$ background is probably explained by the observation that *Tp53* ablation was per se sufficient to grant remarkable growth advantage to liver organoids (Fig. S3C).

Liver organoids expressing FGFR2 fusions generate cholangiocarcinoma upon transplantation in NOD-SCID mice

Control and FF-expressing organoids were transplanted in NOD-SCID mice, either in the liver sub-capsular region or subcutaneously (s.c.). Control organoids were not tumorigenic, as reported[8,9]. Instead, allotransplants of F-BICC1 and F-TACC3 organoids yielded tumors at both orthotopic and s.c. transplantation sites (Fig. 2A, B), with 100% penetrance (Fig. 2C).

Growth of liver tumors led to progressive health deterioration of recipient mice, eventually requiring their euthanasia. These neoplastic lesions (Fig. 2D and Fig. S4A) were diagnosed as moderately to poorly differentiated Ck19^{+}/HepPar1^{-} adenocarcinomas (Fig. 2E, F and S4B-E). Tumor cells were often Ki67^{+} and expressed FGFR2 fusions, as documented by either anti-MYC tag or anti-FGFR2 stain (Fig. 2E, F and S4B, C). Stromal cells were not stained by anti-tag antibodies, an indication of their host origin. Tumors that developed at s.c. injection sites (Fig. 2D and Fig. S4A) were histologically and immuno-phenotypically similar to liver neoplastic lesions (Fig. 2F and Fig. S4C), which implies that F-BICC1 and F-TACC3 liver organoids possessed the molecular information sufficient to drive CCA development also outside the liver district.

Compared to normal liver and regardless of their anatomical site, CCA lesions showed higher expression of a transcriptional signature associated to embryonic cholangiocellular specification, while exhibiting down-regulation of genes linked to hepatocellular lineage determination[19] (Fig. 2G and S5A). A similar pattern was observed when we focused on transcription factors (TF) the

expression of which is regulated during hepatoblast differentiation[19] (Fig. 2H and S5B). Interestingly, we noticed that highly upregulated TF genes in tumor samples included effectors of the Notch (*Sox4*, *Sox9*, *Hey1*) and Yap/Taz (*Tead1* and *Tead4*) pathways (Table S5), which are genetically required for cholangiocytic lineage specification and bile duct morphogenesis[20-22]**.** In line, Notch and Yap/Taz transcriptional signatures were upregulated in FF-driven murine iCCA, compared to normal liver (Fig. 2I and S5C). These data indicate that FGFR2 fusions drive oncogenic conversion of liver bipotent precursors along the cholangiocellular lineage.

Intrahepatic cholangiocarcinoma contains a rich stroma[2]. Indeed, tumor cells in FF-driven mouse tumors were encircled by a collagen-rich stroma (highlighted by Masson's stain in Fig. 2E and S4B) containing anti-α−SMA immunoreactive cells (Fig. S4D, E) - most likely identifiable as cancer associated fibroblasts (CAFs)[2] - and $CD31^+$ vascular endothelial cells (data not shown). When compared to normal liver, tumors were markedly enriched in transcriptional signatures identifying CAFs and liver vascular endothelial cells specifically associated to tumors (LVECt)[23] (Fig. 3A, B and S6A, B), as well as their prototypic functions, that is extracellular matrix deposition/organization/remodeling (CAFs, Fig. 3A and S6A, C) and angiogenesis (LVECt, Fig. 3B and S6B). FF-driven tumors were also enriched for expression of many growth factors and cytokines, with F-BICC1 and F-TACC3 tumors showing partially distinct profiles (Fig. 3C). Interestingly, *Tgfb1* and *Tgfb3*, along with *Ltbp1-3* (which encode Tgfb binding proteins[24]), scored among the top upregulated genes in the growth factor/chemokines signatures (Table S5), indicating that Tgfb signaling could also drive CCA stromal reaction[2] in our model.

In order to address similarities between our model and human FF-driven iCCA, we analyzed RNA-seq data from the human iCCA cancer genome atlas (TCGA) cohort[25]. We found that a number of transcriptional signatures were significantly up/down-regulated in FF^+ compared to FF^- samples (Table S6). FF^+ human iCCA samples were associated with higher activity of well-known cancer-relevant pathways, including epithelial-mesenchymal transition (EMT), KRAS and TGFB

signaling. We observed a similar picture in murine tumors, as shown by single sample gene set variation analysis (GSVA). The only exception was that our murine iCCA models did not show prominent up-regulation of interferon-dependent signatures (Fig. 3D), a likely consequence of murine tumors having thrived in the NOD-SCID immuno-deficient context[26]. Interferon signaling is a prominent driver of cancer immuno-editing[27], which, along with the potential generation of neoantigens spanning sequences around the fusion breakpoint[28], raises the question whether immunotherapeutic approaches could be effective against FF^+ iCCA. We also interrogated our RNA-seq data to search for possible differences between iCCA lesions driven by different FFs. Interestingly, F-BICC1- and F-TACC3-driven murine tumors tended to group separately from each other (Fig. S6D). In aggregate, the above data point to a) relevant similarities between our murine model and human FF^+ iCCA as a whole; b) transcriptional differences generated by individual FGFR2 fusions, potentially linked to biological diversification.

F-MGEA5 expressing organoids were not tumorigenic when transplanted in the liver, even after a 190-day follow-up (Fig. S7A) and yielded *bona fide* iCCA-like lesions in only 1/8 s.c. injection sites (Fig. 2C and S7B-C). In the remaining seven s.c. transplantation sites, we observed the development of cystadenomas lined by dysplastic epithelium. These cystic lesions lacked signs of overt neoplastic transformation, except in one case in which we observed an area showing clear progression to cystic adenocarcinoma (Fig. S7D). We note that the low tumorigenic potential of F-MGEA5-expressing organoids was unlikely to be caused by poor expression/activation of F-MGEA5 itself, which, in fact, was as good as that of F-TACC3 (Fig. 1C). Furthermore, the expression/activation of F-MGEA5 in the single iCCA-like tumor we obtained was comparable to that of F-TACC3-driven tumors (Fig. S7E), implying that F-MGEA5-dependent tumorigenicity did not require selection for super-high levels F-MGEA5 expression/activation.

Cellular models derived from iCCA lesions are addicted to oncogenic signaling by FGFR2 fusions

We derived tumor organoids (henceforth referred to as tumoroids)[29] and conventional 2D cell lines from liver and s.c. tumors expressing F-BICC1 and F-TACC3. Individual tumoroids and 2D cell lines expressed the expected FF, which displayed constitutive catalytic activation (Fig. 4A and S8A), and the Ck19 biliary cell marker (Fig. S8B). As already observed in FF-transduced organoids, F-BICC1 expression was lower than that of F-TACC3 in tumoroids and 2D cell lines. Notably, F-BICC1 displayed a higher stoichiometry of Y657/Y658 phosphorylation compared to F-TACC3 (Fig. 4A and S8A), suggesting that its relatively low expression was compensated for by a high level of intrinsic tyrosine kinase activity. BGJ398 caused dose-dependent suppression of tumoroid growth/viability (Fig. 4B, C), with IC_{50} values in the low nM range. Similar results were obtained with 2D cell lines (Fig. 4D, E and S8C). Thus, murine tumors derived from oncogenic transformation of liver organoids acquired oncogenic addiction to FF signaling.

Next, we investigated signaling cascades downstream to FFs in iCCA cell lines. We focused on the Ras-Erk pathway, because previous work highlighted its potential relevance downstream to FFs[6] and our RNA-seq data pointed to upregulation of the KRAS-driven transcriptional program in human and mouse FF^+ iCCA (Fig. 3D). The docking/scaffolding Frs2 adaptor protein was phosphorylated on tyrosine residues responsible for the recruitment of Grb2 and Shp2[30] (Fig. 5A and S9A-C). Shp2 was phosphorylated on Tyr residues involved in Grb2 binding[25] (Fig. 5A and S9A-C). Tyr phosphorylation of Frs2 and Shp2 correlated with the activating phosphorylation of Mek1/2 and Erk1/2 (Fig. 5A and S9A). All of the above phosphorylation events required FF catalytic activity, because they were suppressed by BGJ398 (Fig. 5A and S9A-C). These data fit in the currently accepted model of FGFR2 activation[31] and support that FFs drive Ras-Erk activation by instructing formation of activity-dependent molecular complexes involving Frs2, Shp2 and Grb2[31] upstream of RAS. In line, pharmacological inhibition of Shp2 by SHP099[32] caused a remarkable reduction of Erk1/2 activation downstream to both F-BICC1 and F-TACC3 (Fig. 5B). It

is notable that inhibition of the FF-Erk1/2 signaling axis by BGJ398 was durable, with no apparent evidence of late pathway reactivation (Fig. 5A and S9A). The protracted signal inhibition achieved by BGJ398 in the above cellular models is congruent with the potent activity exhibited by BGJ398 in cell viability/growth assays (Fig. 4B-E).

Erk1/2 is a necessary signaling hub downstream to FGFR2 fusions in iCCA

Trametinib[33], a clinically approved MEK1/2 inhibitor, suppressed growth/viability of iCCA tumoroids (Fig. 5C, D) and 2D cell lines (Fig. S10A, B), in fact phenocopying BGJ398. In line, the SHP2 inhibitor SHP099 was also effective in curbing growth/viability of F-BICC1-addicted iCCA cells (Fig. S10C, D). We also generated an iCCA model driven by the BGJ398-resistant FGFR2-TACC3 V565F[5] mutant (Fig. 2C and S11A-D) and determined that the resulting F-TKI resistant tumoroids (Fig. S11E, F) were also dependent on Erk1/2 signaling (Fig. S11G).

The above data support a model whereby Erk1/2 activation plays a necessary role in shaping addiction of iCCA cells to FF oncogenic signaling. If so, reactivation of signal flow through the Ras-Erk pathway should rescue FF-driven iCCA cells from BGJ398 inhibition. Indeed, epidermal growth factor (EGF) was able to alleviate BGJ398-mediated growth inhibition in F-TACC3 tumoroids. However, the addition of trametinib strongly reduced EGF-dependent rescue (Fig. 5E and S10E), implying that the EGF signal rescued BGJ398-treated cells through bypass activation of Ras-Erk.

Oncogenic signaling of FGFR2 fusions in iCCA cells is highly sensitive to combined blockade of FGFR2 fusions and Mek1/2

Simultaneous blockade of an oncogenic driver and its required downstream effector/s has been shown to be more efficacious than isolated inhibition of the oncodriver itsel[34,35]. Therefore, we hypothesized that the efficacy of FF targeting could be improved by combining FF blockade with Mek1/2 inhibition. As shown in Fig. 6A-C, BGJ398 and trametinib interacted synergistically in *in*

vitro assays measuring growth/viability of F-BICC1 and F-TACC3 iCCA cellular models. At the biochemical level, synergy between BGJ398 and trametinib correlated with stronger inhibition of cyclin D1 expression and marked induction of cleaved Parp1 (Fig. 6D).

Therapeutic targeting of FGFR2-BICC1-driven iCCA by the BGJ398 + trametinib combination

For *in vivo* validation of the above results, we set out to compare the efficacy of single agent BGJ398 or trametinib versus the BGJ398 + trametinib (B+T) combination in immuno-deficient mice carrying tumors generated by subcutaneous injection of F-BICC1 tumoroids. Pharmacodynamic studies indicated that the B+T combination elicited stronger inhibition of pErk immunoreactivity in comparison to single agents (Fig. S12A; lack of suitable reagents prevented evaluation of pFGFR, see Fig. S13A, B). This was associated to stronger cell killing activity elicited by B+T in comparison to single agents (Fig. S12A). In line, the therapeutic efficacy of the B+T combination was superior to that of single agent BGJ398 already at day 15 and persisted until day 22. Trametinib alone exerted marginal activity (Fig. S12B). However, two sudden deaths occurred in the B+T group between day 20 and 21, despite the fact that BGJ398 and trametinib were used at doses reported in the literature[36,37] and daily animal inspection coupled to body weight measurements (Fig. S12C) had not raised suspicion of overt toxicity.

Because adverse events in the B+T group imposed a degree of caution in the interpretation of the above findings, we carried out a second experiment (henceforth referred to as experiment #2, to distinguish it from experiment #1 presented in Fig. S12), in which the dose of both BGJ398 and trametinib was reduced by 20% in the B+T group; furthermore, B+T was administered according to a de-escalation protocol (5 days/week in the first week, 4 days/week in the second week). In line with experiment #1, we observed rapid tumor growth in the control group and marginal benefit from single agent trametinib. The B+T combination outperformed single agent BGJ398 at the day 15 time-point (Fig. 7A). When therapeutic responses of individual mice were evaluated using

RECIST 1.1-like criteria adapted to experimentation in the mouse[38], we determined that 100% of B+T tumors achieved a partial response (PR) at nadir, compared to 60% in the BGJ398 group (Fig. 7B). Therapeutic responses were associated with increased stroma (most likely generated by reactive fibrosis) and acquisition of a more differentiated glandular phenotype, particularly in B+T tumors; in line, cholangiocellular identity was preserved, as determined by anti-Ck19 reactivity (Fig. 7C and S14A).

Aiming to prolong therapeutic benefit beyond the day 15 time-point, we opted for an adaptive trial strategy, as follows. Average tumor growth on day 15 in the BGJ398 group was comparable to that observed in experiment #1 and therefore indicative of therapeutic resistance (Fig. 7D: note that the burgundy dotted line, reported as reference, corresponds to the BGJ398 group in Fig. S12B). Considering the superior efficacy of the B+T combo, these mice were randomized to receive B+T (as detailed in Fig. S14B), either twice a week (B/B+T-1) or five days a week (B/B+T-2). B+T provided therapeutic benefit in both subgroups, causing tumor growth to level off abruptly and eventually intersect that of mice receiving B+T *ab initio* (Fig. 7D: compare the two B/B+T subgroups with the BGJ398 group dotted line; see also Fig. S14D-E).

Mice in the upfront B+T group were divided in subgroups B+T-1 and B+T-2, based on their performance status (see Fig. S14B, C for details). Mice in the B+T-1 subgroup received no further therapy, while the B+T-2 subgroup was assigned to continue B+T twice a week. Tumor growth remained under control in both subgroups until day 19 (which in the B+T-1 subgroup corresponded to a remarkable eight-day drug-free interval), but it resumed thereafter (Fig. 7D-E). The experiment was stopped on day 22, because most mice had developed skin ulcerations at the tumor site. Thus, the B+T combo afforded better and more prolonged control of tumor growth also in experiment #2, in which no deaths were recorded.

We investigated therapeutic targeting of F-BICC1-driven iCCA also in an orthotopic transplantation setting. In preliminary pharmacodynamic experiments performed on a small number of mice, we observed that the B+T combo yielded the most pervasive suppression of pErk immunolabeling also

in intrahepatic tumors (Fig. 8A). Compared to single agent BGJ398, B+T caused significantly higher tumor cell killing (as assessed by TUNEL assay) with dying cells accumulating in the lumina of glandular structures (Fig. 8A). B+T also trended towards better growth suppression (Ki67 stain), although this did not reach statistical significance (Fig. 8A). B and B+T inhibited angiogenesis to a similar extent (Fig. S15A). Given the marginal activity of trametinib in the above assays and results obtained with s.c. tumors, we omitted its evaluation in efficacy studies, in which luc-directed bioluminescence was used as a proxy for intravital assessment of tumor growth. Again, B and B+T provided clear therapeutic benefit. The B+T combo trended towards higher therapeutic efficacy than single agent BGJ398 (Fig. 8B and S15B). Although this trend did not reach statistical significance in the average tumor growth comparison between the B and B+T groups, RECIST-like evaluation at the endpoint indicated that a single animal (12.5%) in the BGJ398 group had stable disease (SD), whereas the remaining seven mice (87.5%) had progressive disease (PD). In contrast, PD was observed in 55.5% of mice assigned to B+T therapy, with the remaining animals showing either partial response (PR, 11.1%) or SD (33.3%) (Fig. S15B).

Discussion

We have shown that mouse p53-null liver organoids engineered to express a highly recurrent (i.e. F-BICC1) or sporadic (i.e. F-TACC3) FGFR2 fusion generated tumors upon orthotopic or subcutaneous transplantation in immuno-compromised mice. We have extended this conclusion to *Tp53*-null liver organoids expressing FGFR2-CCDC6 (F-CCDC6), yet another FGFR2 fusion reported to occur in iCCA[3,4] (Fig. 2C and S16A-C). Because the primary structure of different human FFs shows a degree of divergence from colinear mouse protein sequences, we opted for not using the syngeneic C57BL/6J strain in tumorigenic assays. However, considering that the immunogenicity of neoantigens generated by gene fusion events in human tumors is HLA-A, B, C restricted[28] and more than sixty genes have been identified thus far as FGFR2 fusion partners in iCCA[4], the exploitation of an immunocompetent mouse model for pursuing translationally relevant studies on the immunobiology of FF-driven iCCA appears to be of limited value.

Tumors were diagnosed as CCA, based on histological and immunophenotypic criteria. In line, they expressed transcriptional signatures associated to cholangiocellular specification/identity, while showing repression of hepatocyte-specific transcriptional programs (Fig. 2G, H and S5A, B). Upregulated signaling pathways included those regulated by Notch, Yap/Taz and Tgfb (Fig. 2I and S5C), which are genetically required for cholangiocytic lineage determination in the embryo[20-22]. It is therefore likely that these pathways are implicated in cholangiocytic specification of bipotent liver precursors transformed by FGFR2 fusions. It remains unclear whether biliary lineage commitment in our iCCA model is a fully cell autonomous program, possibly reflective of the role played by FGFs in biliary cell specification[21], or instead requires tumor cell extrinsic cues. It was recently shown that cytokines released by immune cells activated by necroptotic hepatocytes were required to mediate cholangiocellular conversion of oncogene-expressing mouse hepatocytes[39]. This immune-mediated mechanism was not observed in SCID mice, due to lack of effector immune cells[39], and therefore is unlikely to account for oncogenic biliary lineage specification in our model.

The tumorigenic process instructed by FGFR2 fusions was accompanied by the organization of a stromal reaction, most likely orchestrated by cooption of CAFs by CCA cells[2]. Recent scRNA-seq studies highlighted that, among the different cell types populating the iCCA TME, CAFs produced the largest number of ligands - either soluble or ECM-associated - for receptors expressed by tumor cells[23]. Future studies will have to address whether CAFs play any obligatory role in oncogenic conversion and/or biliary specification of FF-expressing liver organoids.

We observed that structurally different FFs diverged in terms of oncogenic potential. The gradient of FF tumorigenic potency (Fig. 2C) correlated with tumor growth kinetics, because F-CCDC6 and F-MGEA5 s.c. lesions developed at a slower pace than F-BICC1 and F-TACC3 tumors (compare Fig. 2B with Fig. S7B and S16B). The notion that structural diversity among FFs may impact on their biology was also supported by the observation that gene expression patterns of F-BICC1- and F-TACC3-driven tumors tended to cluster independently from each other.

The above data point to a degree of so far unappreciated heterogeneity among iCCA FFs, at least in a p53-null background. Complementing this observation, a recent study reported that FGFR2-AHCYL1 was tumorigenic when expressed in *Cdkn2a*-null mouse liver organoids, but not in *Tp53*$^{-/-}$ background[9]. Therefore, it is possible that FF-driven iCCA pathogenesis might be influenced by the genetic background generated by loss of a specific tumor suppressor gene on one side and still unclear biological properties intrinsic to individual FFs on the other.

Through *in vitro* studies, we identified Ras-Erk as a necessary effector pathway downstream to FFs. Addiction of FF^{+} murine iCCA cells to Ras-Erk signaling is in line with: a) data pointing to up-regulation of KRAS-driven transcriptional signatures in FF^{+} human iCCA (Fig. 3D); b) KRAS and BRAF acting as oncogenic drivers in human iCCA[1]; c) FGFR2 fusions being mutually exclusive with either *BRAF* or *KRAS* mutations[14]. Trametinib interacted synergistically with BGJ398 in iCCA cellular models driven by F-BICC1, F-TACC3 (Fig. 6A, B) and F-CCDC6 (Fig. S16D-F), with the B+T combination exerting more potent cell killing activity when compared to single agents. These

data converge upon the emerging paradigm that simultaneous blockade of multiple components of an oncogenic signaling axis provides for stronger pathway inhibition[35].

The above *in vitro* results informed pharmacologic studies in mice bearing iCCA-like lesions generated by transplantation of F-BICC1 tumoroids. Pharmacodynamic experiments confirmed that the B+T combination inhibited Erk activation more effectively than single agents and had higher cell killing activity, in both s.c. and orthotopic tumors. In line, upfront B+T treatment in the s.c. setting afforded a more pronounced and significantly longer control of tumor growth in comparison to single agent BGJ398. A trend towards increased efficacy of the B+T combo over single agent BGJ398 was observed also in the orthotopic model, particularly when therapeutic response in individual mice, rather than average tumor growth in each experimental group, was used as a metric of therapeutic efficacy. The advantage offered by the B+T combo in our experiments must be considered also in light of the observation that *TP53* mutations are associated to an aggressive disease course and less favorable responses to single agent FGFR TKis in iCCA with *FGFR2* rearrangements[4,16]. While additional studies will be necessary to determine optimal dosing/scheduling of the B+T combo in our iCCA model and evaluate potential differences in therapeutic responses caused by loss of specific TSGs[4,40], we anticipate that translation of our data to clinical experimentation will be facilitated by the available knowledge about the toxicity profiles and biodistribution of clinically advanced F-TKIs and FDA-approved MEK1/2 inhibitors.

An interesting observation was that B+T mitigated therapeutic resistance in mice that progressed while being treated with single agent BGJ398 (Fig. 7D). In assigning these mice to receive B+T treatment, we explicitly assumed that resistance to BGJ398 was caused by the activity of collateral pathway/s capable of driving Erk1/2 signaling in the face of FF blockade, a scenario in line with the abundant expression of growth factors revealed by CCA RNA-seq analyses (Fig. 3C).

Finally, our finding that FF^+ iCCA cells expressing FGFR2-TACC3 V565F remained dependent on Ras-Erk signaling suggests that upfront treatment with the B+T combo may hold the potential to

delay the emergence of resistant clones carrying mutations in the FF TKD[5,6]. This hypothesis is in line with recent pre-clinical studies on tumors driven by NTRK fusions[34].

Conclusions

We have shown that liver organoids can be engineered to model FF-driven iCCA in immunodeficient mice. We envision that this relatively facile model will a) increase our understanding of both tumor cell-intrinsic and -extrinsic determinants of FF-driven iCCA pathogenesis; b) advance pre-clinical experimentation on FF therapeutic targeting.

Acknowledgements

We dedicate our work to the cherished memory of our friends and colleagues Daniela and Marianna, who fought courageously against cancer, and to the Italian Public Health System professionals who operate at the frontline of the Covid-19 epidemic. We are grateful to B. Artegiani, L. Cantley, H. Clevers, M. Huch, H. Liu, K. Meyer, L. Monteonofrio, A. Saborowski, E. Salvati, S. Soddu, F. Spinella, P. Zizza and our colleagues at the Regina Elena Institute for advice and reagents. R. Fraioli and A. Petricca provided excellent technical and secretarial support, respectively. We thank S. Alemà and G. Blandino for critical reading of the manuscript. O.S. is funded by AIRC (IG2018, ID 21627, PI Segatto Oreste) and an intramural grant-in-aid funded by the Italian Ministry of Health.

Figure legends

Fig. 1. **Expression of FGFR2 fusions in mouse liver organoids.** (A) Passage 12 (P12) mouse liver organoids derived from C57BL/6J mice with the indicated *Tp53* genotype were infected with either empty (Ctr) or F-TACC3 encoding retrovirus. Cells were plated in 3D conditions under puromycin selection and photographed at the indicated timepoints. Where required, organoids were passaged at day 7-8, in which case day 10 pictures refer to passage 13 (P13). Scale bar: 100 μm. (B) Organoids transduced with control (Ctr) and FF-encoding recombinant retrovirus were imaged by anti-MYC tag immunostaining or GFP fluorescence (green); actin was visualized by phalloidin (red) and nuclei by DAPI stain. Scale bar: 100 μm. (C) Cell lysates obtained from the indicated *Tp53*$^{-/-}$ organoids were probed with the indicated antibodies. Because steady state expression levels of F-BICC1 were lower than those of other FFs, unambiguous detection of F-BICC1 required loading of more lysate and blotting with anti-MYC antibody (right panel). (D) *Tp53*$^{-/-}$ liver organoids were infected with retrovirus encoding human FGFR2IIIb. Cells were kept in growth factor deprived medium for 2 hours before stimulation with either carrier (-) or 100 ng/ml FGF10 for the indicated time in presence of 5 μg/ml heparin. Lysates from F-TACC3 organoids were run as control. Immunoblot analysis was carried out with the indicated antibodies.

Fig. 2. **Generation of cholangiocarcinomas in mice transplanted with liver organoids expressing FGFR2 fusions.** (A) Growth of liver implants of Ctr, F-BICC1 (F-B) and F-TACC3 (F-T) organoids was imaged by longitudinal live measurement of luciferase activity. The intensity of bioluminescence was color-coded and plotted over time (right panel). (B) Growth of tumors derived from s.c. implantation of Ctr and FF-expressing organoids was monitored by longitudinal caliper measurements. (C) Tumorigenicity score of Ctr and FF-expressing *Tp53*$^{-/-}$ liver organoids. Tumor growth was assessed for each of intrahepatic or s.c. injection sites in individual animals. Note that the characterization of FGFR2-CCDC6 (F-CCDC6) organoids and F-CCDC6-driven CCA lesions is presented in the Discussion and reported in Fig. S16. (D) Representative images of liver (left) and

subcutaneous (right) tumors obtained upon transplantation of F-BICC1 liver organoids. (E) Histopathology of liver tumors obtained upon intrahepatic (i.h.) transplantation of F-BICC1 organoids. Tissue sections were stained as indicated. Red dotted lines demarcate the boundary between tumor (Ck19^{+}, HepPar1^{-}) and normal liver (HepPar1^{+}). The MYC stain identifies MYC-tagged F-BICC1. Collagen fibers appear as blue-colored areas in Masson's trichrome stain. (F) Histopathology of tumors obtained upon s.c. transplantation of F-BICC1 liver organoids. Sections were stained as indicated. (G) Average expression – from RNA-seq data in adult liver (L) and FF-driven tumors (T) expressing F-BICC1 or F-TACC3 - of gene sets associated to differentiation of mouse embryonal hepatoblasts into cholangiocytes (top) and hepatocytes (bottom)[19]. See also Fig. S5A. (H) Same as in panel G, except that signatures contained solely genes encoding transcription factors (TF) upregulated during embryonal specification of cholangiocytes (top) and hepatocytes (bottom)[19]. See also Fig. S5B. (I) Average expression from RNA-seq data of gene sets associated to Notch (Molecular Signature Database, MSigDB) and Yap/Taz[41] activation in adult normal liver (L) and FF-driven iCCA (T). See also Fig. S5C. G-I: P values indicated on top of each panel were inferred by Student's t-test.

Fig. 3. **Transcriptional analysis of cholangiocarcinomas.** (A) Average expression from RNA-seq of gene sets identifying iCCA CAFs[23] and CAF-associated functions (col stands for collagen). L, liver; T, tumors. See also Fig. S6A, C. (B) Average expression of gene sets identifying liver vascular endothelial cells associated to liver tumors (LVECt)[23] and angiogenesis. See also Fig. S6B. (C) Average expression from RNA-seq (left) and hierarchical clustering of standardized expression (right) of the MSigDB gene set encompassing 452 genes encoding growth factors and cytokines. L/1 and L/2 correspond to two independent mouse liver samples. F-BICC1 (F-B) and F-TACC3 (F-T) tumors are labelled by a numeric code; the numeric code is followed by a letter (A or B) to identify independent tumors arising in the same animal. A-C: P values indicated on top of each panel were inferred by Student's t-test. (D) Gene set enrichment of RNA-seq profiles from human iCCA (left and middle plots) and murine iCCA driven by either F-BICC1 or F-TACC3 (right plot).

Boxplots depict GSVA activity scores of significantly upregulated gene sets in FF^+ versus FF^- human iCCA. Red boxes refer to FF^+ tumors (whether human or murine), blue boxes indicate FF^- human iCCA.

Fig. 4. Cellular models derived from iCCA lesions are addicted to FF signaling. (A) Immunoblot analysis of F-BICC1 (F-B) and F-TACC3 (F-T) expression/activation in tumoroids derived from iCCA lesions. Tum 2 and Tum 3-5 were derived from liver lesions, Tum 1 and 6 from s.c. lesions. Total cell lysates were probed with the indicated antibodies. (B, C) Dose-dependent profile of growth inhibition in BGJ398-treated F-BICC1 (B) and F-TACC3 (C) tumoroid cultures. Cell growth was assayed after 72 hours of drug treatment using the CellTiter-Glo kit and plotted as % decrease of luminescence over untreated cells. IC_{50} values are indicated for each tumoroid. Representative photographs of Tum 1 (B) and Tum 4 (C) were taken at the 72-hour endpoint using Incucyte S3 Live-Cell Imaging System. (D, E) Same as in B, C except that 2D cell lines (CL) derived from F-BICC1 (panel D: CL1 and CL2) and F-TACC3 (panel E: CL3 and CL4) were used.

Fig. 5. **FF-driven iCCA cells are dependent on downstream Ras-Erk activity**. (A) F-BICC1 (F-B) and F-TACC3 (F-T) iCCA cell lines were treated with the indicated concentrations of BGJ398 for 6 and 30 hours before lysis. Total cell extracts were immunoblotted to identify the indicated total and phosphorylated signaling proteins. Anti β-actin reactivity was used to normalize for total protein loading. (B) F-BICC1 and F-TACC3 iCCA cell lines were incubated for 4 hours with the SHP2 inhibitor SHP099. Total cell extracts were immunoblotted as indicated. (C, D) F-BICC1 (C) and F-TACC3 (D) tumoroids were exposed to escalating concentrations of trametinib for 72 hours. Cell growth/viability was assessed as detailed in Fig. 4B, C using CellTiter-Glo. IC_{50} values are indicated for each tumoroid. Representative photographs of Tum 1 (B) and Tum 4 (C) were taken at the 72-hour endpoint using Incucyte S3 Live-Cell Imaging System. (E) F-TACC3 tumoroid cells (Tum 3) were grown -/+ EGF (10 ng/ml) in presence or absence of BGJ398 (B, 25 nM), trametinib (T, 25 nM) or their combination (B+T). Cell growth was measured with the CellTiter-Glo kit. Note that EGF enhanced cell proliferation in drug-untreated cells. See also Supplementary Fig. 10E. Data

are presented as mean ± SEM. One-way analysis of variance (ANOVA) with a post hoc Bonferroni's test was used to evaluate statistical significance among the indicated treatments (**P = 0.009).

Fig. 6. **Improved targeting of FF oncogenic dependence by combined FF and Mek1/2 blockade**. (A, B) The combination index (CI) for the BGJ398 + trametinib combination was calculated according to Chou-Talalay, as detailed in Supplementary materials and methods. Values <1 indicate synergistic drug interaction. A and B show data obtained with tumoroids Tum 1 (F-BICC1) and Tum 4 (F-TACC3), respectively. (C) F-BICC1 (CL1, top) and F-TACC3 (CL4, bottom) 2D cell lines were treated with BGJ398 and trametinib, either as single agents or in combination. Cells were stained with crystal violet. (D) Semi-confluent monolayers of the indicated F-BICC1 (F-B) and F-TACC3 (F-T) cell lines were treated with the indicated drugs for 30 or 48 hours before lysis. Total cell lysates were immunoblotted as indicated.

Fig. 7. **An adaptive trial approach to therapeutic targeting of F-BICC1 tumors**. (A) Tumor bearing mice were treated with the indicated drugs and average tumor volumes from each experimental group were plotted over time. Groups were composed as follows: vehicle n = 6, trametinib n = 6, BGJ398 n = 10, B+T n = 10. Data are presented as mean ± SEM. Two-tailed unpaired t-test was used to evaluate significant differences between BGJ398 and B+T groups (****P <0.0001 on day 15). (B) The spaghetti plot shows individual responses (tumor volume changes), evaluated according to RECIST1.1-like criteria, in mice assigned to either BGJ398 or B+T treatment. PD, progressive disease (≥35% increase from baseline); PR, partial response (≤50% reduction from baseline); SD: stable disease (intermediate changes from baseline) (C) Tumors explanted on day 15 from mice that underwent the indicated drug treatments were stained with H&E (top row) and Ck19 (bottom row). Scale bar: 30 μm. (D) Adaptive therapeutic treatment of mice belonging to the B and B+T groups (same as in Fig. S12B), which were assigned to the indicated subgroups during the third week of the experiment (highlighted in yellow; the black arrow indicates the start of third week drug treatments). Vehicle and trametinib groups are the same as in

panel 7A and are reported here for reference. The burgundy dotted line refers to single agent BGJ398 group in experiment #1 (Fig. S12B). Subgroups: B/B+T-1 n = 5, B/B+T-2 n = 5, B+T-1 n = 5, B+T-2 n = 5. Data are presented as mean ± SEM. One-way analysis of variance (ANOVA) with a post hoc Bonferroni's test was used to evaluate significant differences in tumor volumes between the indicated subgroups. Differences among the four subgroups in the yellow-shaded area lacked statistical significance (P >0.05 on day 22). (E) RECIST 1.1-like evaluation of individual tumor responses in mice assigned to the B+T-1 and B+T-2 subgroups.

Figure 8. Therapeutic targeting of FGFR2 fusions in orthotopic tumors. (A) Mice carrying tumors obtained by sub-capsular injection of F-BICC1 tumoroids were subjected to daily administration of either vehicle or the indicated drugs for 2 days. Animals were sacrificed 3 hours after the last treatment and explanted livers were processed for histopathology as indicated. Statistical evaluation of $TUNEL^+$ and $Ki67^+$ cells is shown in bar graphs. Data are presented as mean ± SEM. One-way analysis of variance (ANOVA) with a post hoc Bonferroni's test was used to evaluate statistical significance among the indicated groups. (B) Mice carrying tumors generated by sub-capsular injection of F-BICC1 tumoroids were treated with either vehicle (n = 4), BGJ398 (n = 8) and B+T (n = 9), as in experiment presented in Fig.7A. Tumor growth was assessed by measuring bioluminescence of tumor cells in individual mice at the indicated timepoints. Boxplots report median bioluminescence values for each experimental group. One-way analysis of variance (ANOVA) with a post hoc Bonferroni's test was used to evaluate statistical significance among the indicated groups (**P = 0.0014; ***P = 0.0005).

References

Author names in bold designate shared co-first authorship

[1] Lamarca A, Barriuso J, McNamara MG, Valle JW. Molecular targeted therapies: ready for "prime time" in biliary tract cancer. J Hepatol 2020;73:170-185.

[2] Sirica AE, Gores GJ, Groopman JD, Selaru FM, Strazzabosco M, Wei Wang X, et al. Intrahepatic Cholangiocarcinoma: Continuing Challenges and Translational Advances. Hepatology 2019;69:1803-1815.

[3] Wu YM, Su F, Kalyana-Sundaram S, Khazanov N, Ateeq B, Cao X, et al. Identification of targetable FGFR gene fusions in diverse cancers. Cancer Discov 2013;3:636-647.

[4] Silverman IM, Hollebecque A, Friboulet L, Owens S, Newton RC, Zhen H, et al. Clinicogenomic analysis of FGFR2-rearranged cholangiocarcinoma identifies correlates of response and mechanisms of resistance to pemigatinib. Cancer Discov 2020. (online ahead of print).

[5] **Goyal L**, **Saha SK**, Liu LY, Siravegna G, Leshchiner I, Ahronian LG, et al. Polyclonal Secondary FGFR2 Mutations Drive Acquired Resistance to FGFR Inhibition in Patients with FGFR2 Fusion-Positive Cholangiocarcinoma. Cancer Discov 2017;7:252-263.

[6] **Goyal L**, **Shi L**, **Liu LY**, **Fece de la Cruz F**, Lennerz JK, Raghavan S, et al. TAS-120 Overcomes Resistance to ATP-Competitive FGFR Inhibitors in Patients with FGFR2 Fusion-Positive Intrahepatic Cholangiocarcinoma. Cancer Discov 2019;9:1064-1079.

[7] **Krook MA**, **Bonneville R**, Chen HZ, Reeser JW, Wing MR, Martin DM, et al. Tumor heterogeneity and acquired drug resistance in FGFR2-fusion-positive cholangiocarcinoma through rapid research autopsy. Cold Spring Harb Mol Case Stud 2019;5:a004002.

[8] **Saborowski A**, **Wolff K**, Spielberg S, Beer B, Hartleben B, Erlangga Z, et al. Murine Liver Organoids as a Genetically Flexible System to Study Liver Cancer. Hepatol Commun 2019;3:423-436.

[9] **Ochiai M**, **Yoshihara Y**, **Maru Y**, Tetsuya M, Izumiya M, Imai T, et al. Kras-driven heterotopic tumor development from hepatobiliary organoids. Carcinogenesis 2019;40:1142-1152.

[10] Artegiani B, van Voorthuijsen L, Lindeboom RGH, Seinstra D, Heo I, Tapia P, et al. Probing the Tumor Suppressor Function of BAP1 in CRISPR-Engineered Human Liver Organoids. Cell Stem Cell 2019;24:927-943.e926.

[11] **Sun L**, **Wang Y**, Cen J, Ma X, Cui L, Qiu Z, et al. Modelling liver cancer initiation with organoids derived from directly reprogrammed human hepatocytes. Nat Cell Biol 2019;21:1015-1026.

[12] **Prior N**, **Inacio P**, Huch M. Liver organoids: from basic research to therapeutic applications. Gut 2019;68:2228-2237.

[13] **Broutier L**, **Andersson-Rolf A**, **Hindley CJ**, Boj SF, Clevers H, Koo BK, et al. Culture and establishment of self-renewing human and mouse adult liver and pancreas 3D organoids and their genetic manipulation. Nat Protoc 2016;11:1724-1743.

[14] Lowery MA, Ptashkin R, Jordan E, Berger MF, Zehir A, Capanu M, et al. Comprehensive Molecular Profiling of Intrahepatic and Extrahepatic Cholangiocarcinomas: Potential Targets for Intervention. Clin Cancer Res 2018;24:4154-4161.

[15] **Borad MJ**, **Champion MD**, **Egan JB**, Liang WS, Fonseca R, Bryce AH, et al. Integrated genomic characterization reveals novel, therapeutically relevant drug targets in FGFR and EGFR pathways in sporadic intrahepatic cholangiocarcinoma. PLoS Genet 2014;10:e1004135.

[16] Jain A, Borad MJ, Kelley RK, Wang Y, Abdel-Wahab R, Meric-Bernstam F, et al. Cholangiocarcinoma with FGFR genetic aberrations: a unique clinical phenotype. JCO Precision Oncology; 2018:1-12.

[17] Lamberti D, Cristinziano G, Porru M, Leonetti C, Egan JB, Shi CX, et al. HSP90 Inhibition Drives Degradation of FGFR2 Fusion Proteins: Implications for Treatment of Cholangiocarcinoma. Hepatology 2019;69:131-142.

[18] Javle M, Lowery M, Shroff RT, Weiss KH, Springfeld C, Borad MJ, et al. Phase II Study of BGJ398 in Patients With FGFR-Altered Advanced Cholangiocarcinoma. J Clin Oncol 2018;36:276-282.

[19] **Yang L**, **Wang WH**, **Qiu WL**, Guo Z, Bi E, Xu CR. A single-cell transcriptomic analysis reveals precise pathways and regulatory mechanisms underlying hepatoblast differentiation. Hepatology 2017;66:1387-1401.

[20] **Poncy A**, **Antoniou A**, Cordi S, Pierreux CE, Jacquemin P, Lemaigre FP. Transcription factors SOX4 and SOX9 cooperatively control development of bile ducts. Dev Biol 2015;404:136-148.

[21] Ober EA, Lemaigre FP. Development of the liver: Insights into organ and tissue morphogenesis. J Hepatol 2018;68:1049-1062.

[22] Lee DH, Park JO, Kim TS, Kim SK, Kim TH, Kim MC, et al. LATS-YAP/TAZ controls lineage specification by regulating TGFβ signaling and Hnf4α expression during liver development. Nat Commun 2016;7:11961.

[23] Massalha H, Bahar Halpern K, Abu-Gazala S, Jana T, Massasa EE, Moor AE, et al. A single cell atlas of the human liver tumor microenvironment. Mol Syst Biol 2020;16:e9682.

[24] Rifkin DB, Rifkin WJ, Zilberberg L. LTBPs in biology and medicine: LTBP diseases. Matrix Biol 2018;71-72:90-99.

[25] Farshidfar F, Zheng S, Gingras MC, Newton Y, Shih J, Robertson AG, et al. Integrative Genomic Analysis of Cholangiocarcinoma Identifies Distinct IDH-Mutant Molecular Profiles. Cell Rep 2017;18:2780-2794.

[26] Zaidi MR. The Interferon-Gamma Paradox in Cancer. J Interferon Cytokine Res 2019;39:30-38.

[27] Vidal P. Interferon α in cancer immunoediting: From elimination to escape. Scand J Immunol 2020;91:e12863.

[28] **Yang W**, **Lee KW**, **Srivastava RM**, Kuo F, Krishna C, Chowell D, et al. Immunogenic neoantigens derived from gene fusions stimulate T cell responses. Nat Med 2019;25:767-775.

[29] Broutier L, Mastrogiovanni G, Verstegen MM, Francies HE, Gavarró LM, Bradshaw CR, et al. Human primary liver cancer-derived organoid cultures for disease modeling and drug screening. Nat Med 2017;23:1424-1435.

[30] Gotoh N. Regulation of growth factor signaling by FRS2 family docking/scaffold adaptor proteins. Cancer Sci 2008;99:1319-1325.

[31] Turner N, Grose R. Fibroblast growth factor signalling: from development to cancer. Nat Rev Cancer 2010;10:116-129.

[32] Chen YN, LaMarche MJ, Chan HM, Fekkes P, Garcia-Fortanet J, Acker MG, et al. Allosteric inhibition of SHP2 phosphatase inhibits cancers driven by receptor tyrosine kinases. Nature 2016;535:148-152.

[33] Samatar AA, Poulikakos PI. Targeting RAS-ERK signalling in cancer: promises and challenges. Nat Rev Drug Discov 2014;13:928-942.

[34] **Cocco E**, **Schram AM**, Kulick A, Misale S, Won HH, Yaeger R, et al. Resistance to TRK inhibition mediated by convergent MAPK pathway activation. Nat Med 2019;25:1422-1427.

[35] **Misale S**, **Bozic I**, Tong J, Peraza-Penton A, Lallo A, Baldi F, et al. Vertical suppression of the EGFR pathway prevents onset of resistance in colorectal cancers. Nat Commun 2015;6:8305.

[36] **Kitai H**, **Ebi H**, Tomida S, Floros KV, Kotani H, Adachi Y, et al. Epithelial-to-Mesenchymal Transition Defines Feedback Activation of Receptor Tyrosine Kinase Signaling Induced by MEK Inhibition in KRAS-Mutant Lung Cancer. Cancer Discov 2016;6:754-769.

[37] **Bockorny B**, **Rusan M**, Chen W, Liao RG, Li Y, Piccioni F, et al. RAS-MAPK Reactivation Facilitates Acquired Resistance in FGFR1-Amplified Lung Cancer and Underlies a Rationale for Upfront FGFR-MEK blockade. Mol Cancer Ther 2018;17:1526-1539.

[38] Corso S, Isella C, Bellomo SE, Apicella M, Durando S, Migliore C, et al. A Comprehensive PDX Gastric Cancer Collection Captures Cancer Cell-Intrinsic Transcriptional MSI Traits. Cancer Res 2019;79:5884-5896.

[39] **Seehawer M**, **Heinzmann F**, D'Artista L, Harbig J, Roux PF, Hoenicke L, et al. Necroptosis microenvironment directs lineage commitment in liver cancer. Nature 2018;562:69-75.

[40] **Ding H**, **Zhao J**, Zhang Y, Yu J, Liu M, Li X, et al. Systematic Analysis of Drug Vulnerabilities Conferred by Tumor Suppressor Loss. Cell Rep 2019;27:3331-3344.e3336.

[41] Cordenonsi M, Zanconato F, Azzolin L, Forcato M, Rosato A, Frasson C, et al. The Hippo transducer TAZ confers cancer stem cell-related traits on breast cancer cells. Cell 2011;147:759-772.

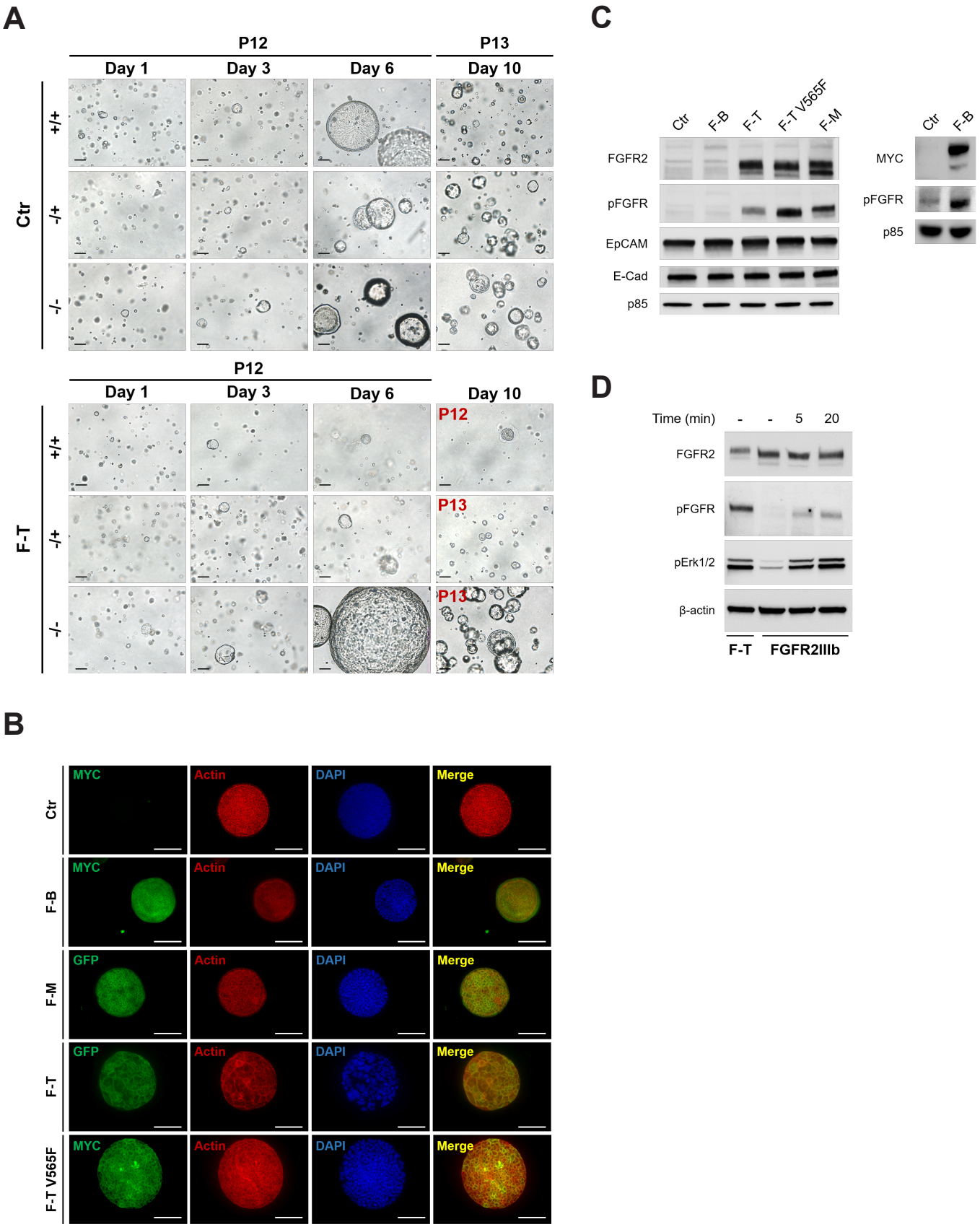
A
P12
P13
Day 1
Day 3
Day 6
Day 10
Ctr
+/+
-/+
-/-
F-T
P12
P13
B
MYC
Actin
DAPI
Merge
GFP
Ctr
F-B
F-M
F-T
F-T V565F
C
Ctr
F-B
F-T
F-T V565F
F-M
FGFR2
pFGFR
EpCAM
E-Cad
p85
MYC
D
Time (min)
-
-
5
20
FGFR2
pFGFR
pErk1/2
β-actin
F-T
FGFR2IIIb

Figure 1

A

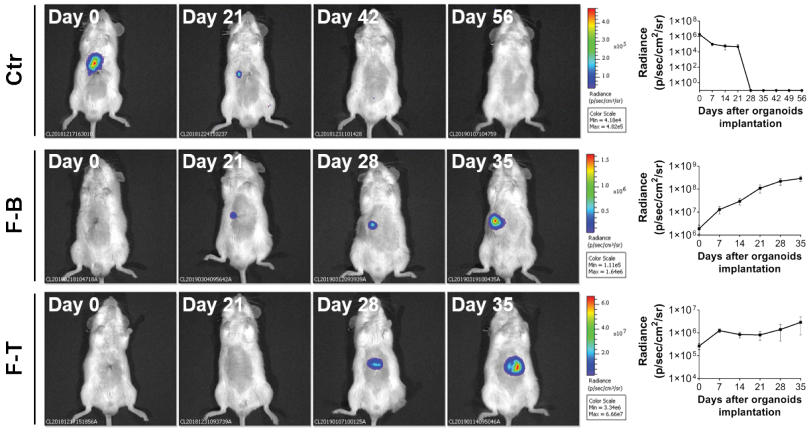

B

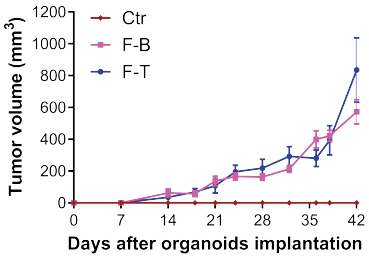

C

Groups	intrahepatic	subcutaneous
Ctr	0/6	0/8
F-BICC1	4/4	4/4
F-MGEA5	0/4	1/8
F-TACC3	7/7	4/4
F-TACC3 V565F	2/2	4/4
F-CCDC6	n.d.	6/8

D

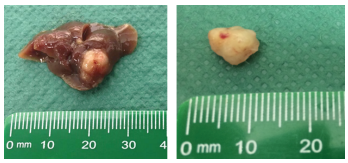

E

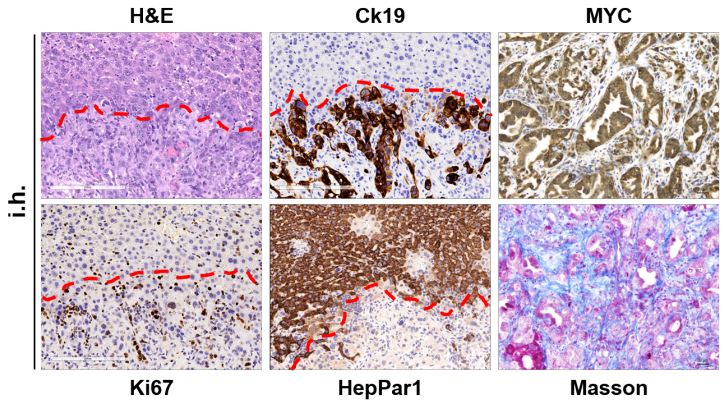

F

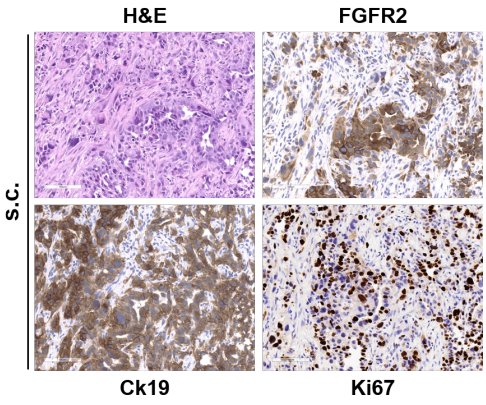

G

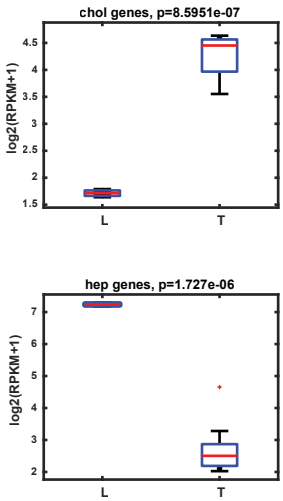

H

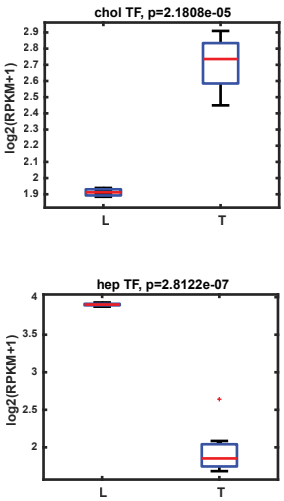

I

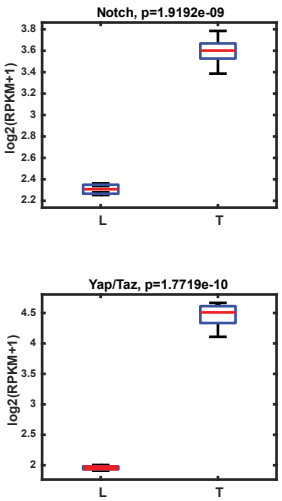

Figure 2

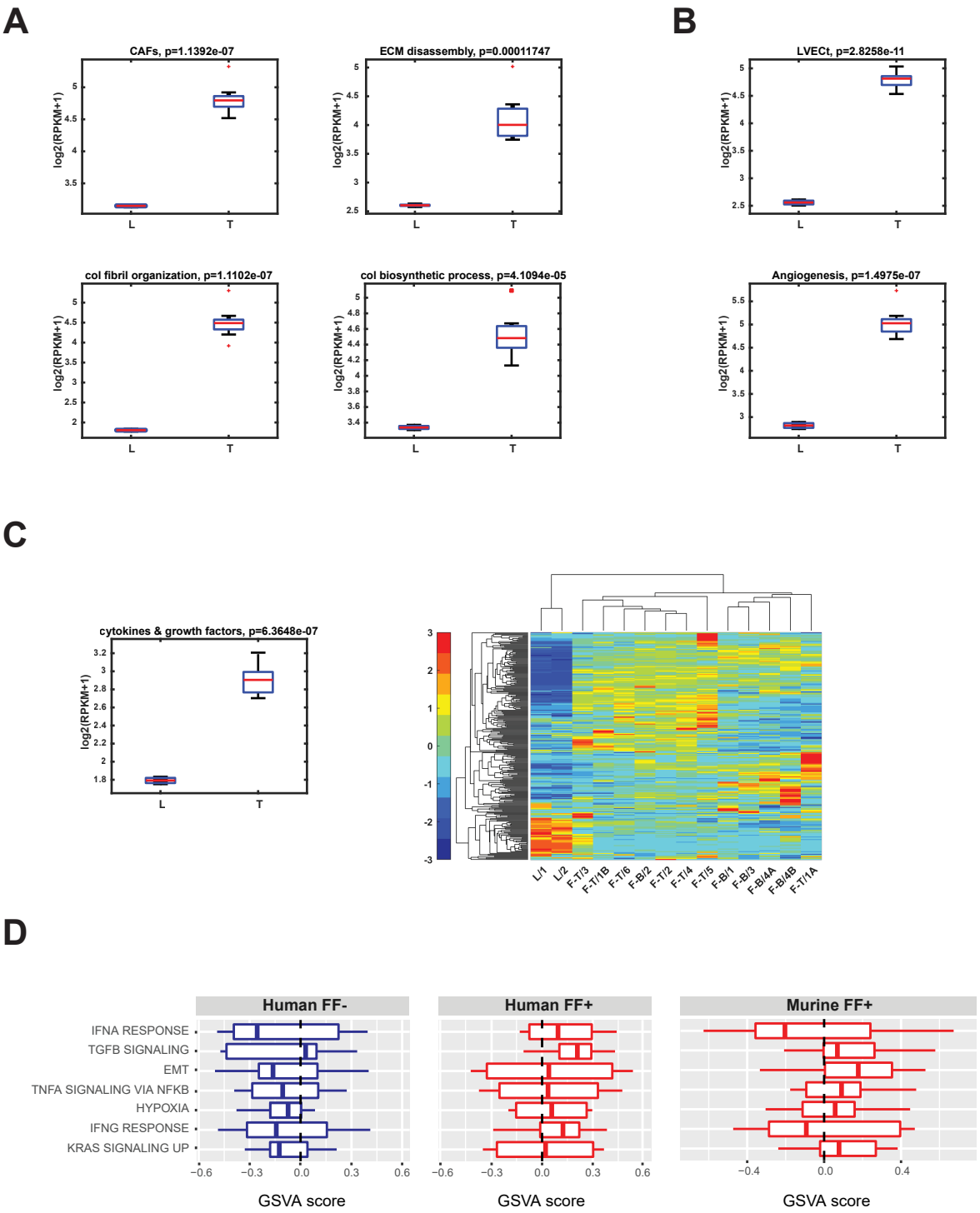
A
CAFs, p=1.1392e-07
ECM disassembly, p=0.00011747
col fibril organization, p=1.1102e-07
col biosynthetic process, p=4.1094e-05
B
LVECt, p=2.8258e-11
Angiogenesis, p=1.4975e-07
log2(RPKM+1)
L
T
C
cytokines & growth factors, p=6.3648e-07
L/1
L/2
F-T/3
F-T/1B
F-T/6
F-B/2
F-T/2
F-T/4
F-T/5
F-B/1
F-B/3
F-B/4A
F-B/4B
F-T/1A
D
Human FF-
Human FF+
Murine FF+
IFNA RESPONSE
TGFB SIGNALING
EMT
TNFA SIGNALING VIA NFKB
HYPOXIA
IFNG RESPONSE
KRAS SIGNALING UP
GSVA score

Figure 3

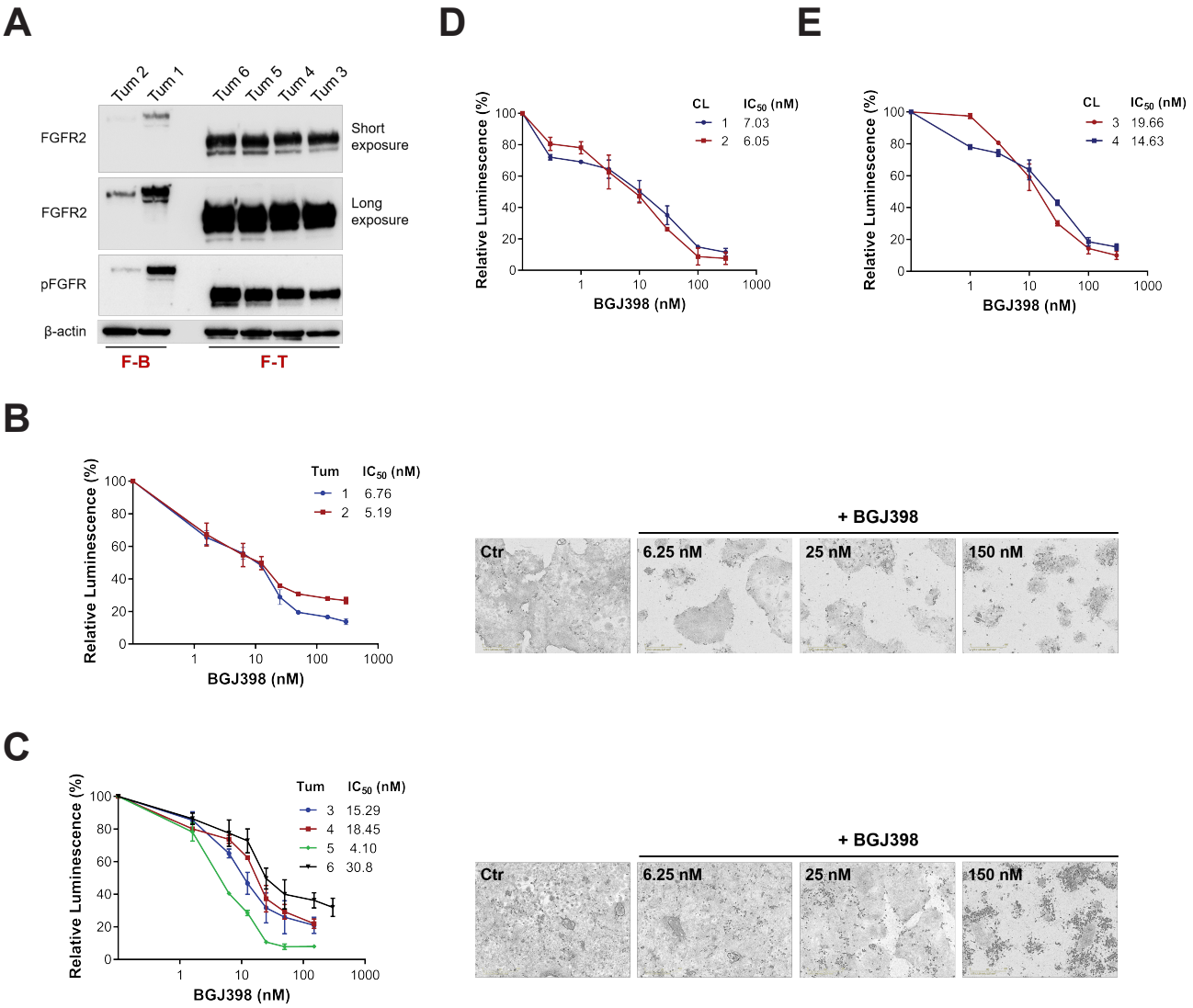
A
Tum 2
Tum 1
Tum 6
Tum 5
Tum 4
Tum 3
FGFR2
Short exposure
FGFR2
Long exposure
pFGFR
β-actin
F-B
F-T
D
Relative Luminescence (%)
BGJ398 (nM)
CL IC50 (nM)
1 7.03
2 6.05
E
Relative Luminescence (%)
BGJ398 (nM)
CL IC50 (nM)
3 19.66
4 14.63
B
Relative Luminescence (%)
BGJ398 (nM)
Tum IC50 (nM)
1 6.76
2 5.19
+ BGJ398
Ctr
6.25 nM
25 nM
150 nM
C
Relative Luminescence (%)
BGJ398 (nM)
Tum IC50 (nM)
3 15.29
4 18.45
5 4.10
6 30.8
+ BGJ398
Ctr
6.25 nM
25 nM
150 nM

Figure 4

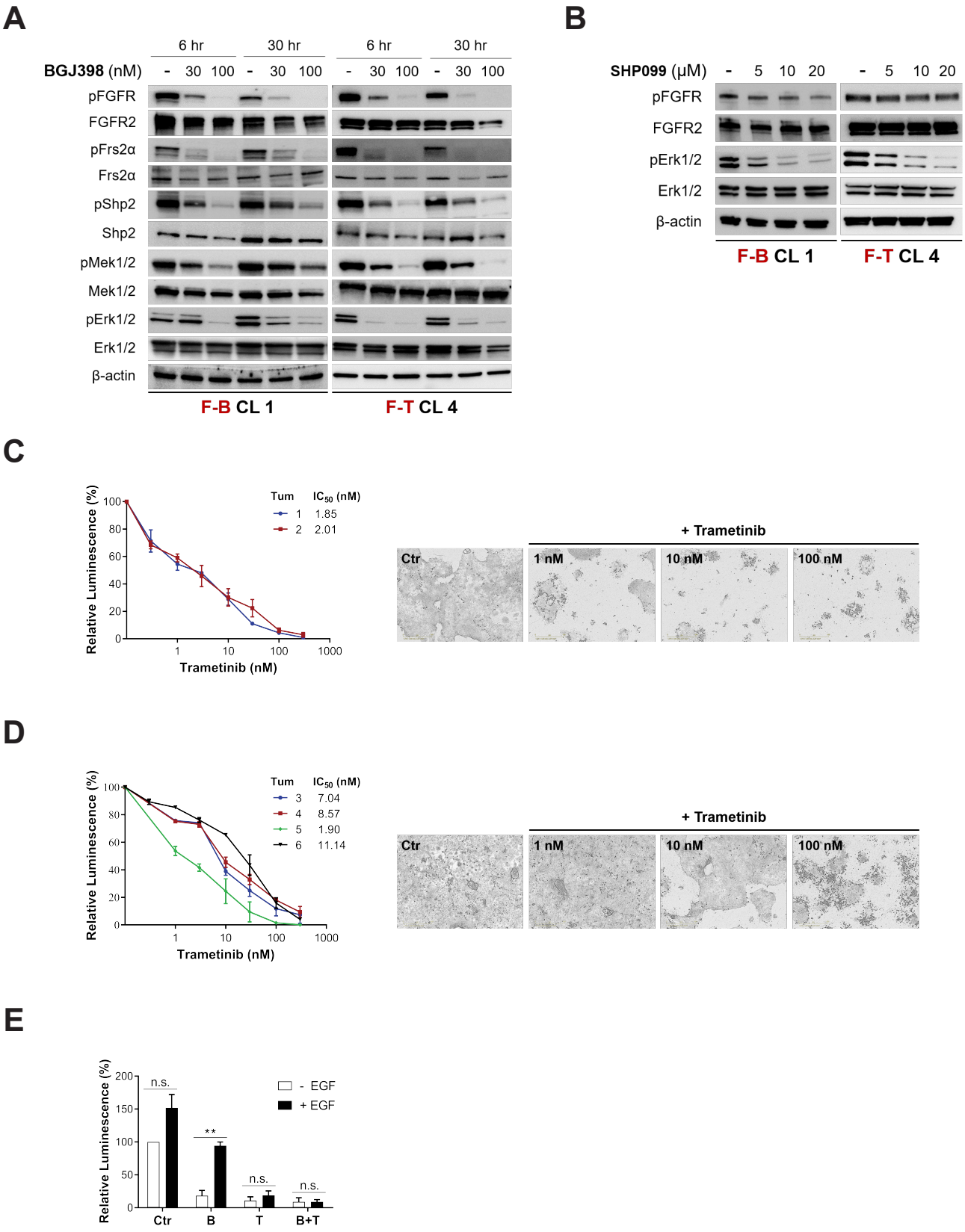
A
6 hr
30 hr
6 hr
30 hr
BGJ398 (nM)
- 30 100 - 30 100 - 30 100 - 30 100
pFGFR
FGFR2
pFrs2α
Frs2α
pShp2
Shp2
pMek1/2
Mek1/2
pErk1/2
Erk1/2
β-actin
F-B CL 1
F-T CL 4
B
SHP099 (μM)
- 5 10 20 - 5 10 20
pFGFR
FGFR2
pErk1/2
Erk1/2
β-actin
F-B CL 1
F-T CL 4
C
Relative Luminescence (%)
Trametinib (nM)
Tum IC50 (nM)
1 1.85
2 2.01
+ Trametinib
Ctr
1 nM
10 nM
100 nM
D
Relative Luminescence (%)
Trametinib (nM)
Tum IC50 (nM)
3 7.04
4 8.57
5 1.90
6 11.14
+ Trametinib
Ctr
1 nM
10 nM
100 nM
E
Relative Luminescence (%)
n.s.
**
n.s.
n.s.
- EGF
+ EGF
Ctr
B
T
B+T

Figure 5

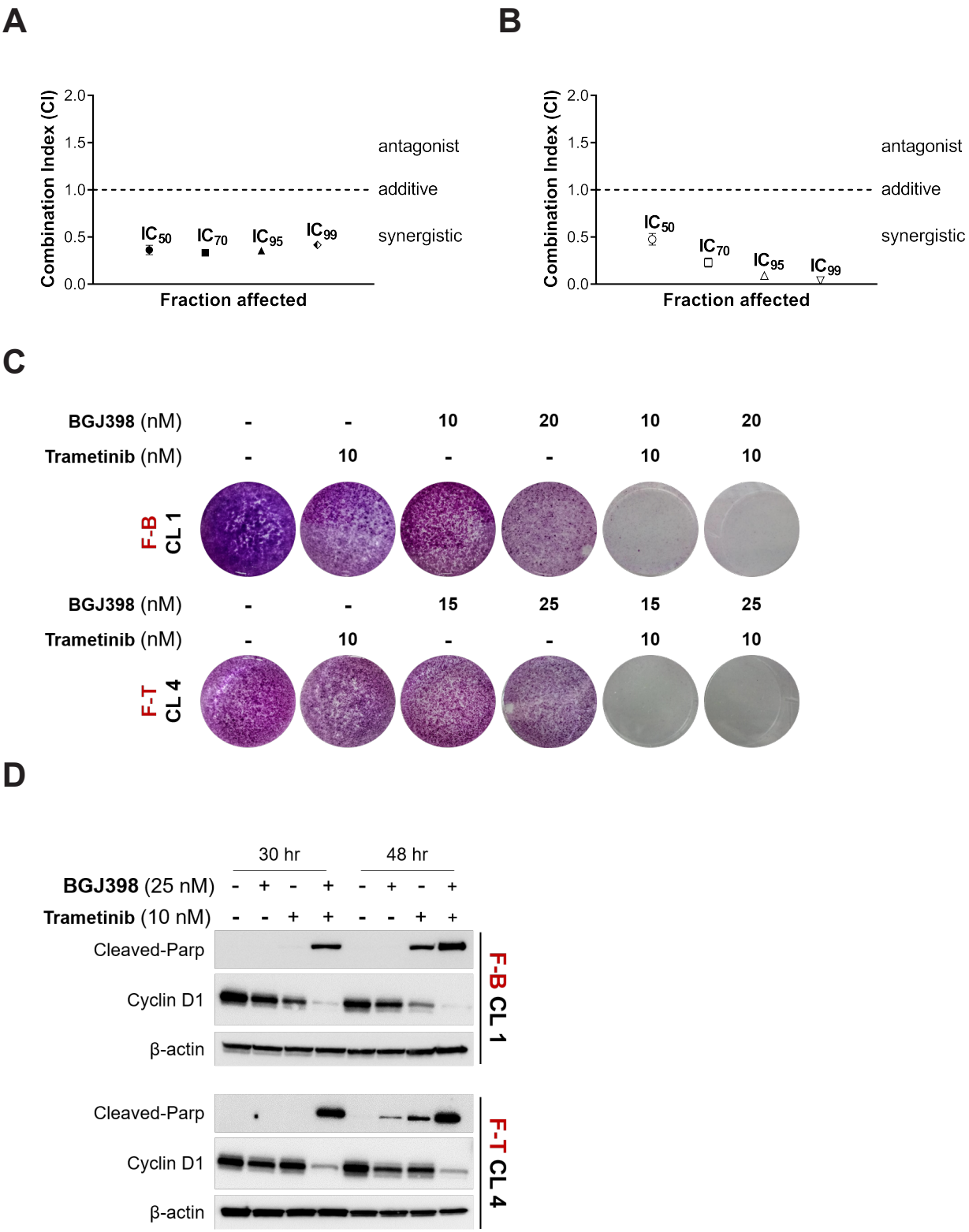
A
B
Combination Index (CI)
2.0
1.5
1.0
0.5
0.0
antagonist
additive
synergistic
IC50
IC70
IC95
IC99
Fraction affected
C
BGJ398 (nM) - - 10 20 10 20
Trametinib (nM) - 10 - - 10 10
F-B CL 1
BGJ398 (nM) - - 15 25 15 25
Trametinib (nM) - 10 - - 10 10
F-T CL 4
D
30 hr
48 hr
BGJ398 (25 nM) - + - + - + - +
Trametinib (10 nM) - - + + - - + +
Cleaved-Parp
Cyclin D1
β-actin
F-B CL 1
F-T CL 4

Figure 6

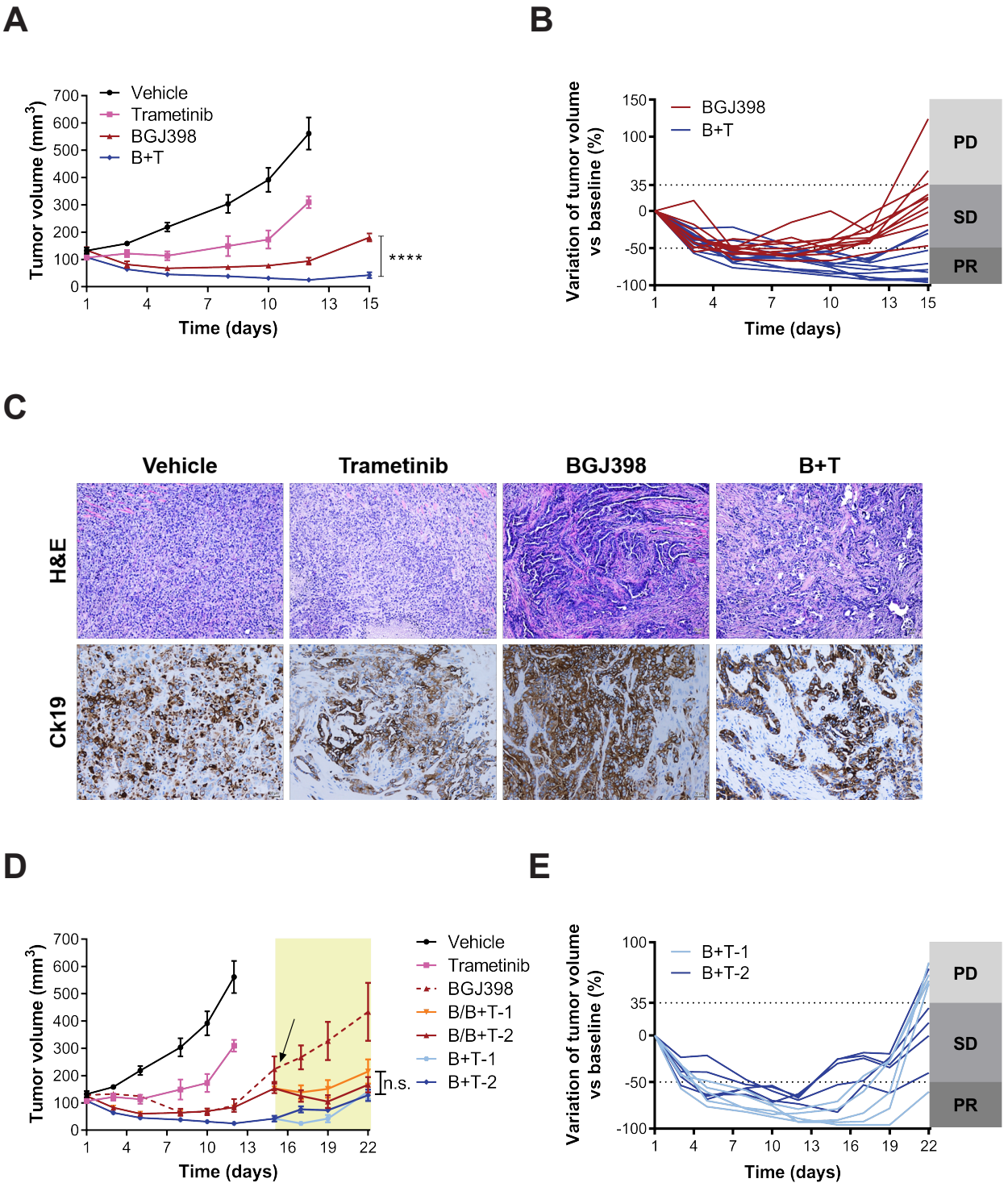
A
Vehicle
Trametinib
BGJ398
B+T
Tumor volume (mm3)
Time (days)
****
B
BGJ398
B+T
Variation of tumor volume vs baseline (%)
PD
SD
PR
Time (days)
C
Vehicle
Trametinib
BGJ398
B+T
H&E
Ck19
D
Vehicle
Trametinib
BGJ398
B/B+T-1
B/B+T-2
B+T-1
B+T-2
n.s.
Tumor volume (mm3)
Time (days)
E
B+T-1
B+T-2
Variation of tumor volume vs baseline (%)
PD
SD
PR
Time (days)

Figure 7

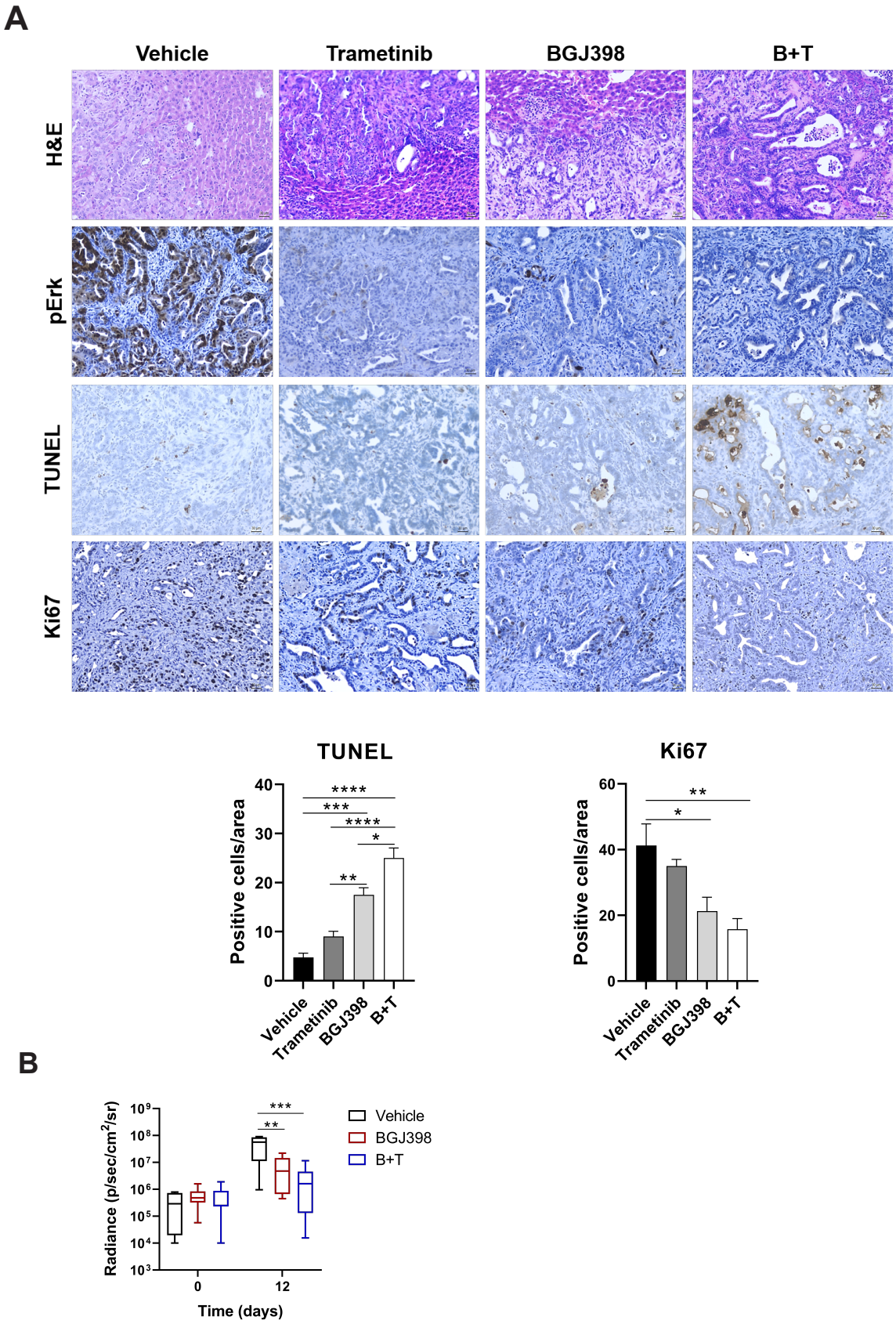
A
Vehicle
Trametinib
BGJ398
B+T
H&E
pErk
TUNEL
Ki67
TUNEL
Positive cells/area
Vehicle
Trametinib
BGJ398
B+T
Ki67
Positive cells/area
B
Radiance (p/sec/cm²/sr)
Time (days)
Vehicle
BGJ398
B+T

Figure 8